UC San Diego
UC San Diego Previously Published Works

Title

An Endplate-Based Joint Coordinate System for Measuring Kinematics in Normal and Abnormally-Shaped Lumbar Vertebrae.

Permalink

Journal

ISSN

Authors

Berry, David B
Rodríguez-Soto, Ana E
Tokunaga, Jana R
et al.

Publication Date

DOI

Peer reviewed

An Endplate-Based Joint Coordinate System for Measuring Kinematics in Normal and Abnormally-Shaped Lumbar Vertebrae

David B. Berry,[1] **Ana E. Rodríguez-Soto,**[1] **Jana R. Tokunaga,**[2] **Sara P. Gombatto,**[2] **and Samuel R. Ward**[1]

[1]University of California San Diego; [2]San Diego State University

Vertebral level-dependent, angular, and linear translations of the spine have been measured in 2D and 3D using several imaging methods to quantify postural changes due to loading conditions and tasks. Here, we propose and validate a semiautomated method for measuring lumbar intervertebral angles and translations from upright MRI images using an endplate-based, joint coordinate system (JCS). This method was validated using 3D printed structures, representing intervertebral discs (IVD) at predetermined angles and heights, which were positioned between adjacent cadaveric vertebrae as a gold standard. Excellent agreement between our measurements and the gold standard was found for intervertebral angles in all anatomical planes (ICC > .997) and intervertebral distance measurements (ICC > .949). The proposed endplate-based JCS was compared with the vertebral body-based JCS proposed by the International Society of Biomechanics (ISB) using the 3D printed structures placed between 3 adjacent vertebrae from a cadaver with scoliosis. The endplate-based method was found to have better agreement with angles in the sagittal plane (ICC = 0.985) compared with the vertebral body-based method (ICC = .280). Thus, this method is accurate for measuring 3D intervertebral angles in the healthy and diseased lumbar spine.

Keywords: lumbar spine, posture, intervertebral angle, upright MRI, scoliosis

Load carriage, tasks, and pathology have been shown to alter lumbar spine posture.[1,2] High-resolution studies have quantified the kinematics of the lumbar spine in vitro, however the effect of active muscles and passive soft tissue tension are difficult to replicate,[3] which makes their correlation to the in vivo condition questionable. In vivo vertebral posture changes have been measured using computerized tomography (CT),[4] biplanar radiography,[5] magnetic resonance imaging (MRI),[6,7] and combinations of multiple imaging modalities.[8] The development of upright MRI machines has allowed for the study of in vivo postural changes in the bony elements and soft tissues of the spine in relevant and functional positions. Therefore, images acquired using upright MRI include the effects of gravity, muscle activity, motor control, pain, and pathology on the body's posture. Several upright MRI studies of the lumbar spine have focused on only midsagittal angular and translational changes.[7,9] The kinematic behavior of the intervertebral joint in the axial and coronal planes is often omitted, although altered biomechanical behavior of the spine has been associated with low back pain and other pathologies.[3] Therefore, quantifying spine three-dimensional (3D) biomechanical behavior is crucial for understanding the progression of the aging and load-related pathology in the lumbar spine.

In 2002, the International Society of Biomechanics (ISB) proposed a standard joint coordinate system (JCS) for the spine[10]—similar to JCSs used to study the lumbar spine[3,11]—to facilitate comparisons among various studies of the spine, including abnormally-shaped vertebrae that present in scoliosis. The ISB JCS is centered within the body of each vertebra in the spine, and is based on distinct anatomical landmarks. However, a vertebral body-based approach may not accurately reflect intervertebral angles when vertebrae are nonnormal in shape, as is frequently observed in pathology. Two studies have used an endplate-based JCS to measure 3D kinematics of the lumbar spine using MRI,[12,13] however the method has not been validated in healthy or pathological conditions. Therefore, the goal of this study was to describe and validate a robust imaging-based method to measure sagittal, coronal, and axial intervertebral angles and distances. To achieve this, we propose a modified endplate-based version of the ISB JCS for the intervertebral joints that allows for accurate measurement of intervertebral angles and distances in 3D. We validated and tested this modified JCS in typically developed and scoliotic cadaveric vertebrae.

Methods

Intervertebral disc models were designed with specified angles and heights at predetermined angles (Figure 1A) and were printed with ABS plastic in 0.01 in (0.025 cm) thick layers using a 3D printer. These models were used as the gold standard for validation of the kinematic measurements in 3 planes of motion: flexion–extension, lateral bending, and axial rotation. Flexion–extension angles ranged from –80° to 80°, in 5° increments from 0° to 40° (and 0º to –40°), and 10° increments from 40° to 80° (and –40° to –80°). Lateral bending angles ranged from –40° (left) to 40° (right) in increments of 5°. Similarly, axial rotation ranged from –15° (left) to 15° (right) in increments of 5°. Additional models were fabricated as gold standards for intervertebral distances; these ranged from 10 mm to 22.5 mm in increments of 2.5 mm, without angulation.

David B. Berry, Ana E. Rodríguez-Soto, and Samuel R. Ward are with the Department of Bioengineering, University of California San Diego, La Jolla, CA. Jana R. Tokunaga and Sara P. Gombatto are with the Doctor of Physical Therapy Program, San Diego State University, San Diego, CA. Samuel R. Ward is also with the Departments of Radiology and Orthopaedic Surgery, University of California San Diego, La Jolla, CA. Address author correspondence to Samuel R. Ward at srward@ucsd.edu.
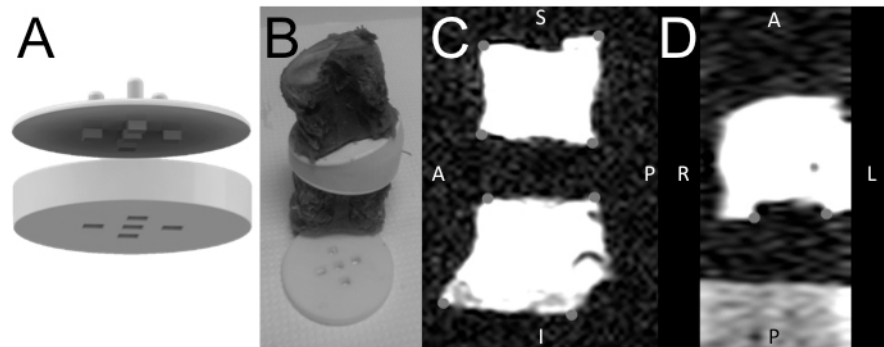
Figure 1 — (A) The 3D printed intervertebral disc model (bottom) and vertebral endplate (top). The endplate model has 5 square pins that press into the holes in the intervertebral disc model, and 3 posts that press into holes drilled into the endplates of the cadaver vertebrae. (B) The vertebra–model–vertebra construct viewed posteriorly. Markers placed on the corners of the vertebrae in sagittal (C) and axially-reformatted (D) T1-weighted magnetic resonance imaging scans.

Four functional spinal units (FSUs) (L2–L3 [n = 2], L3–L4 [n = 2]) were excised from 4 cadavers (80.0 ± 17.6 years, 2 male) to evaluate the accuracy of the proposed method. All soft tissues surrounding the FSUs, including the intervertebral disc (IVD), were removed. The posterior elements were removed midpedicle to allow for supra-physiological range of motion measurements. Three perforations were drilled on the adjacent endplates of 2 vertebrae (ie, inferior endplate of L2 and superior endplate of L3) in an equilateral triangular shape. These perforations allowed for securing printed IVD models to adjacent vertebrae (Figure 1B). All angular and distance IVD models were placed between the 2 vertebrae of each FSU, one at a time, and scanned using an upright MRI scanner. These data were used to validate the angular and distance measurements taken with the proposed method in normally-shaped vertebrae.

To assess the accuracy of both the proposed modification and current ISB JCS definitions on intervertebral joint angular measurements in the presence of pathology, we used 2 adjacent FSUs (L1–L3) excised from a cadaver with left-convexity scoliosis. The L2 vertebra was wedged, sloping down from the right-posterior to left-anterior corner. The superior (L1–L2) and inferior (L2–L3) FSUs were combined and scanned as a stacked construct in multiple known positions. The angular position of the superior FSU (L1–L2) was measured from 5° of flexion to 5° of extension and from 5° of left lateral bending to 5° of right lateral bending, both in 5° increments. The angular position of the inferior FSU (L2–L3) was measured from 10° of flexion to 10° of extension and 10° of left lateral bending to 10° of right lateral bending, in increments of 10°. Angular measurements of the intervertebral joint were taken using the proposed endplate-based JCS and ISB-recommended vertebral body-based JCSs, applied to abnormally-shaped vertebrae.

Each vertebra–model–vertebra construct was scanned with a 0.6-T upright MRI (Fonar Corporation, Melville, NY). Sagittal T1-weighted images (TR: 427 ms, TE: 17 ms, NEX: 1) were obtained with a matrix size of 256 × 256, field of view of 35 cm, thickness of 3 mm, and scan time of 2:30.[6]

Markers were placed on the corners of each vertebra on each sagittal magnetic resonance image (Figure 1C) using OsiriX (Geneva, Switzerland).[14] A second set of markers was placed on each pedicle at the same distance from the posterior vertebral body in axially-reformatted images (Figure 1D). The position of each marker was imported into Matlab (Mathworks, Natick, MA) and postprocessed using custom software to fit planes to both endplates

of each vertebra using principle component analysis (PCA). A right-handed coordinate system was defined for the superior C_s and inferior C_I endplates of each vertebra. The origin of the coordinate system was placed at the geometric centroid of the endplate. The Y-axis was defined as the vector normal to the plane fit to each endplate from the PCA, pointing cephalad. The orientation of the Z-axis was defined as a line parallel to a line connecting markers on the pedicles, projected onto the plane fit to the endplate, with the positive axis pointing to the right. The X-axis was defined as the vector orthogonal to the Y- and Z-axes, pointing anterior (Figure 2). For a given FSU, the rotation matrix (R) between the superior endplate of the inferior vertebra, and the inferior endplate of the superior vertebra, was calculated as $R = C_s \cdot inv (C_I)$. The rotation matrix follows the Y-Z-X convention defined as follows: where θ, ϕ, and ψ are the rotations in radians around the Y-, Z-, and X-axes, respectively.

$$R = R_Y(\theta)\,R_Z(\phi)\,R_X(\psi) = \begin{bmatrix} R_{11} & R_{12} & R_{13} \\ R_{21} & R_{22} & R_{23} \\ R_{31} & R_{32} & R_{33} \end{bmatrix} \quad (1)$$

$$= \begin{bmatrix} \cos\phi\cos\theta & \sin\psi\sin\theta - \cos\psi\cos\theta\sin\phi & \cos\psi\sin\theta + \cos\theta\sin\phi\sin\psi \\ \sin\phi & \cos\phi\cos\psi & -\cos\phi\sin\psi \\ -\cos\phi\sin\theta & \cos\theta\sin\psi + \cos\psi\sin\phi\sin\theta & \cos\psi\cos\theta - \sin\phi\sin\psi\sin\theta \end{bmatrix}$$

The Euler angles that describe the orientation of the superior vertebra with respect to the inferior vertebra are θ, ϕ, and ψ. We solved for the Euler angles θ, ϕ, and ψ from the rotation matrix R and obtained the following:

$$\phi = \sin^{-1}(R_{21}),\ \theta = \sin^{-1}\left(\frac{R_{31}}{-\cos^{-1}(\phi)}\right),\ \psi = \sin^{-1}\left(\frac{R_{23}}{-\cos^{-1}(\phi)}\right) \quad (2)$$

The rotations around each off-plane axis were removed to maintain the true in-plane rotation.

Anterior and posterior intervertebral distances were defined as the Euclidean distance between the centroid of the superior and inferior corners of adjacent vertebra, respectively. Central intervertebral distance was defined as the Euclidean distance between the origins of adjacent endplates.

A power analysis was conducted on pilot data to determine the number of samples needed to observe a correlation between
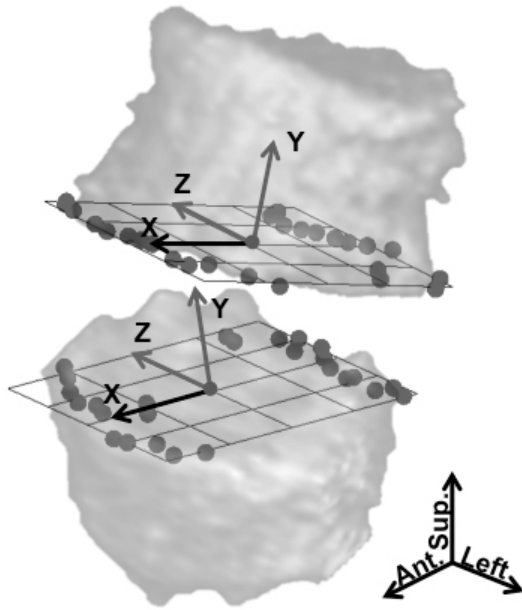
Figure 2 — Joint coordinate systems for adjacent vertebral endplates defined from markers placed on the corners of the vertebrae. The Y-axis is normal to the best-fit plane for the endplate of the vertebrae. The Z-axis is the projection of a line connecting similar landmarks on the pedicles of the vertebra onto the plane. The X-axis is normal to the Y- and Z-axis, pointing anterior.

expected and measured intervertebral angles, which yielded a necessary sample size of 4 ($\rho = 0.98$, $\alpha = .05$, $\beta = 0.20$). The degree of agreement between expected and measured intervertebral angles and IVD distances was assessed using intraclass correlation coefficients (2,1) (ICC[2,1]). For the abnormally-shaped vertebrae, ICC(2,1) were calculated between the gold standard of the intervertebral angles and measurements taken with both the proposed and the ISB JCSs. Average absolute error (AAE) was calculated for each intervertebral angle and intervertebral distance. The coefficient of determination (r^2) was calculated to determine the total variance accounted for by the proposed method. Root mean square error (RMSE) was calculated to determine the magnitude of the error in the measurements. All statistics were performed using SPSS (Version 21, IBM, Armonk, NY). All data are reported as mean ± 95% confidence interval (CI) unless otherwise stated.

Results

In normally-shaped vertebrae, excellent agreement and low absolute error were observed when compared with the gold standard (Table 1, Figure 3). Intervertebral angles in the sagittal, coronal, and axial planes had an ICC > .990, and anterior, center, and posterior intervertebral distance had an ICC > .949. The average absolute errors for the sagittal, coronal, and axial intervertebral angle measurements were 0.77°, 1.34°, and 0.78°, respectively.

In addition, angular positions were measured using the cadaveric vertebrae of 2 adjacent scoliotic FSUs and IVD models of known angles. We found an excellent agreement between the gold standard and measured intervertebral angles using the proposed modification to the ISB JCS in the sagittal and coronal planes for both functional spinal units (ICC > .985; Figure 4A). Axial angles were identical since the Z-axis definition is the same in both JCSs. However, the ISB JCS definition yielded poor agreement between expected and measured intervertebral angles for the superior FSU in the sagittal plane (ICC = .280) and good agreement in the coronal plane (ICC = .896). The intervertebral angle for the superior FSU in the sagittal plane of motion was underestimated by approximately 13° flexion in every position with the ISB JCS definition (Figure 4B). For the inferior FSU, there was excellent agreement between the expected and measured angles using the ISB JCS definitions in the sagittal and coronal planes (ICC > .940).

Discussion

The proposed endplate-based version of the ISB JCS for the intervertebral joint yields accurate measurements of angles and distances in all 3 planes of motion for normally- and abnormally-shaped vertebrae. When the standard ISB JCS was used to measure joint angles in samples with severe shape abnormalities, measurement errors were profound. These errors are due to the fact that the ISB JCS defines the inferior–superior vector by the line that passes through the center of the inferior to the superior endplate, forming a perpendicular vector to the endplate planes only when they are parallel, which is not the case in pathological vertebrae.

There are a few potential limitations to this study. First, markers defining the vertebral body boundaries could have been placed inaccurately on anatomical landmarks. The coefficient of variation (CV) has previously been calculated to investigate intra- and interuser precision using this method;[6] intervertebral angles and distances had a CV of 0.58° and 0.38 mm, respectively. This result, coupled

Table 1   Results of validation of intervertebral angles and intervertebral distances

	Sagittal	Coronal	Axial	Anterior Intervertebral Distance	Center Intervertebral Distance	Posterior Intervertebral Distance
r^2	.999	.995	.990	.947	.946	.942
ICC (95% CI)	1 (1–1)	0.999 (0.998–0.999)	0.997 (0.994–0.999)	0.955 (0.243–0.989)	0.954 (0.229–0.989)	0.949 (0.156–0.988)
RMSE ± SD	0.95° ± 2.16°	1.66° ± 2.12°	1.09° ± 1.63°	1.08 mm ± 2.08 mm	1.10 mm ± 2.08 mm	1.14 mm ± 2.13 mm
AAE ± SD	0.77° ± 0.55°	1.34° ± 1.03°	0.78° ± 0.79°	1.60 mm ± 1.08 mm	1.62 mm ± 1.09 mm	1.74 mm ± 1.13 mm

Abbreviations: ICC = intraclass correlation coefficient; CI = confident interval; RMSE = root mean square error; SD = standard deviation; AAE = average absolute error.
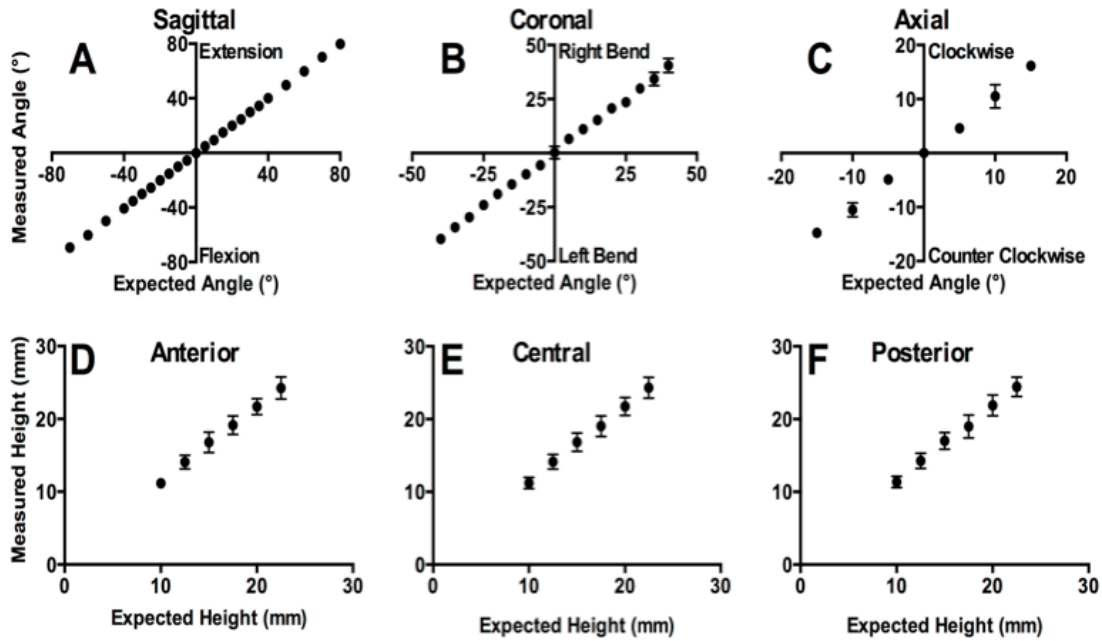
Figure 3 — Measured vs expected sagittal (A), coronal (B), and axial (C) intervertebral angles, and anterior (D), central (E), and posterior (F) disc distances.
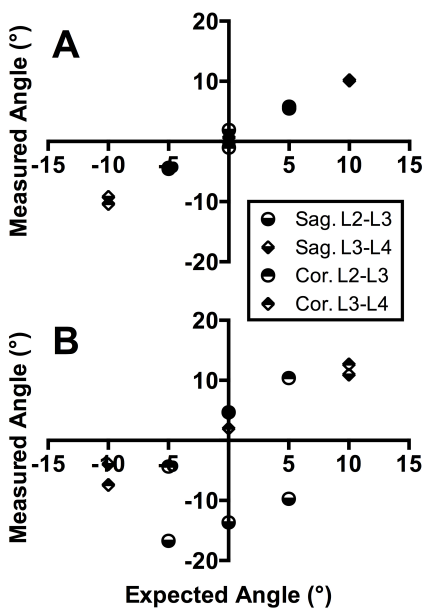

Figure 4 — Scoliotic stacks consisting of 3 vertebrae and 2 intervertebral disc models were scanned at known angles and evaluated using the proposed (A) and International Society of Biomechanics (B) joint coordinate system definitions. Superior (circle) and inferior (triangle) intervertebral angles were measured in the sagittal (bottom filled) and coronal (top filled) planes. Axial measurements were identical between the two joint coordinate systems and are not shown. Data are shown as single measurement. Sag. = sagittal; Cor. = coronal.

with the highly-accurate ICC shown in the study, indicates that anatomical landmark identification does not limit this algorithm's ability to measure intervertebral angles. Second, we chose to validate this algorithm with a clinically-relevant pulse sequence in an upright MRI machine. This pulse sequence has a short scan time to minimize motion artifact and patient pain, resulting in decreased image resolution. While we did not evaluate the influence of voxel dimensions on the accuracy of the algorithm, we suspect accuracy will decline with increasing voxel dimensions. The small lower limit of the 95% CI observed for the height measurements (Table 1) is likely due to the large in-plane voxel dimensions used in this study; the accuracy of distances is limited by in-plane resolution. In addition, the small sample size used decreases the generalizability of the results, particularly for the scoliotic vertebrae. For a case of extreme pathology, the difference between the 2 methods is apparent. However, these techniques will measure the same angle for normally-shaped vertebrae. The relationship between vertebral body deformation and error measuring intervertebral angles using the ISB JCS is unknown and needs further investigation.

The proposed endplate-based modification to the ISB JCS can be used to quantify postural or kinematic changes that occur in the lumbar spine, both in people with healthy and pathologic spines. This study is the first to validate a method of measuring intervertebral angles and distances from MRI images, using an endplate-based JCS and a well-established gold standard. In the future, this approach can be used to study postural changes that result from load, specific tasks, and back pain in patients with normal and abnormal spine morphology.

Acknowledgment

References

1. Jackson RP, McManus AC. Radiographic analysis of sagittal plane alignment and balance in standing volunteers and patients with low back pain matched for age, sex, and size: a prospective

controlled clinical study. *Spine*. 1994;19(14):1611–1618. PubMed doi:10.1097/00007632-199407001-00010

2. Keorochana G, Taghavi CE, Lee KB, et al. Effect of sagittal alignment on kinematic changes and degree of disc degeneration in the lumbar spine: an analysis using positional MRI. *Spine*. 2011;36(11):893–898. PubMed doi:10.1097/BRS.0b013e3181f4d212

3. Panjabi MM, Oxland T, Yamamoto I, Crisco J. Mechanical behavior of the human lumbar and lumbosacral spine as shown by three-dimensional load-displacement curves. *J Bone Joint Surg Am*. 1994;76(3):413–424. PubMed

4. Willén J, Danielson B. The diagnostic effect from axial loading of the lumbar spine during computed tomography and magnetic resonance imaging in patients with degenerative disorders. *Spine*. 2001;26(23):2607–2614. PubMed doi:10.1097/00007632-200112010-00016

5. Glaser DA, Doan J, Newton PO. Comparison of 3-Dimensional spinal reconstruction accuracy: biplanar radiographs with EOS versus computed tomography. *Spine*. 2012;37(16):1391–1397. PubMed doi:10.1097/BRS.0b013e3182518a15

6. Rodríguez-Soto AE, Jaworski R, Jensen A, et al. Effect of load carriage on lumbar spine kinematics. *Spine*. 2013;38(13):E783–E791. PubMed doi:10.1097/BRS.0b013e3182913e9f

7. Shymon S, Hargens AR, Minkoff LA, Chang DG. Body posture and backpack loading: an upright magnetic resonance imaging study of the adult lumbar spine. *Eur Spine J*. 2014;23(7):1407–1413. PubMed doi:10.1007/s00586-014-3247-5

8. Wang S, Passias P, Li G, Li G, Wood K. Measurement of vertebral kinematics using noninvasive image matching method–validation and application. *Spine*. 2008;33(11):E355–E361. PubMed doi:10.1097/BRS.0b013e3181715295

9. Alyas F, Connell D, Saifuddin A. Upright positional MRI of the lumbar spine. *Clin Radiol*. 2008;63(9):1035–1048. PubMed doi:10.1016/j.crad.2007.11.022

10. Wu G, Siegler S, Allard P, et al. ISB recommendation on definitions of joint coordinate system of various joints for the reporting of human joint motion—part I: ankle, hip, and spine. *J Biomech*. 2002;35(4):543–548. PubMed doi:10.1016/S0021-9290(01)00222-6

11. Stokes IA. Three-dimensional terminology of spine deformity. A report presented to the Scoliosis Research Society by the Scoliosis Research Society Working Group on 3-dimensional terminology of spinal deformity. *Spine*. 1994;19(2):236–248. PubMed doi:10.1097/00007632-199401001-00020

12. Li G, Wang S, Passias P, Xia Q, Li G, Wood K. Segmental in vivo vertebral motion during functional human lumbar spine activities. *Eur Spine J*. 2009;18(7):1013–1021. PubMed doi:10.1007/s00586-009-0936-6

13. Passias PG, Wang S, Konzanek M, et al. Segmental lumbar rotation in patients with discogentic low back pain during functional weight-bearing activities. *J Bone Joint Surg Am*. 2011;93(1):29–37. PubMed doi:10.2106/JBJS.I.01348

14. Rosset A, Spadola L, Ratib O. OsiriX: an open-source software for navigating in multidimensional DICOM images. *J Digit Imaging*. 2004;17(3):205–216. PubMed doi:10.1007/s10278-004-1014-6